

## Scattering of flexural wave in a thin plate with multiple circular holes by using the multipole Trefftz method

Lee, W. M.<sup>1</sup>, Chen, J. T.<sup>2</sup>, Zhu, Q. F.<sup>1</sup>, Lin, Y. C.<sup>1</sup>

<sup>1</sup>Department of Mechanical Engineering, China University of Science and Technology

<sup>2</sup>Department of Harbor and River Engineering, National Taiwan Ocean University

<sup>2</sup>Department of Mechanical and Mechatronic Engineering, National Taiwan Ocean University

### Abstract

The scattering of flexural wave by multiple circular holes in an infinite thin plate is analytically solved by using the multipole Trefftz method. The dynamic moment concentration factor (DMCF) along the edge of circular holes is determined. Based on the addition theorem, the solution of the field represented by multiple coordinate systems centered at each circle can be transformed into one coordinate system centered at one circle, where the boundary conditions are given. In this way, a coupled infinite system of simultaneous linear algebraic equations is derived as an analytical model for the scattering of flexural wave by multiple holes in an infinite plate subject to the incident flexural wave. The formulation is general and is easily applicable to dealing with the problem containing multiple circular holes. Although the number of hole is not limited in our proposed method, the numerical results of an infinite plate with three circular holes are presented in the truncated finite system. The effects of both incident wave number and the central distance among circular holes on the DMCF are investigated. Numerical results show that the DMCF of three holes is larger than that of one, when the space among holes is small and meanwhile the specified direction of incident wave is subjected to the plate.

**Keywords:** scattering, flexural wave, plate, dynamic moment concentration factor, addition theorem

## 多極 Trefftz 法求解含多圓形孔洞薄板彎曲波散射

李為民<sup>1</sup>, 陳正宗<sup>2</sup>, 朱全發<sup>1</sup>, 林呈應<sup>1</sup>

<sup>1</sup> 中華科技大學機械工程系

<sup>2</sup> 國立臺灣海洋大學河海工程系、機械與機電工程系

### 摘要

本文利用多極 Trefftz 法以解析的方式求解含多圓形孔洞之無限域薄板彎曲波散射問題，並計算沿孔洞邊界之動應力集中係數(Dynamic Moment Concentration Factor)。根據加法定理，由多個以各個圓孔中心為原點的座標系統所表示的場解可變換成由單一個座標系統表示，而該座標系統所參考的圓孔邊界條件為給定。依此方式可求得一無限耦合線性代數系統作為一個含多圓形孔洞之無限域薄板受入射彎曲波作用的解析模式。本文理論推導具有一般性可推廣至多圓形孔洞問題。雖然本文所提方法在處理圓形孔洞個數沒有限制，在捨去高次的有限項之代數系統中，本文給出含三個圓形孔洞的數值算例，以探討入射波數與圓形孔洞間距等因素對動應力集中係數的影響。數值結果顯示，當圓形孔洞彼此相當接近且入射彎曲波具有特定入射角時，三圓形孔洞的應力集中係數大於單圓形孔洞的結果。

**關鍵詞：** 散射，彎曲波，薄板，動應力集中係數，加法定理

### 1. Introduction

Thin plates with multiple circular holes are widely used in engineering structures, e.g. missiles, aircraft, etc. Geometric discontinuities due to these holes result in the stress concentration, which signi-

ficantly reduce the load carrying capacity. The deformation and corresponding stresses induced by dynamic loading are propagated throughout the structure by means of wave. At the irregular interface of different media, flexural wave scattered

in all directions recursively interacts with the incident wave. It turns out that the scattering of the associated stress wave results in dynamic stress concentrations which are larger than static ones at certain wave frequencies [1].

Nishimura and Jimbo [2] were two pioneers for the analytical study of the dynamic stress concentration and they determined the stresses in the vicinity of a spherical inclusion in the elastic solid under a harmonic force. Pao [3] studied the scattering of flexural waves and dynamic stress concentrations around a circular hole, and proposed an analytical solution. Since then, most research work has focused on the scattering of elastic wave and the resulted dynamic stress concentration and has led to a rapid development of analytical or numerical approach such as the method of wave function expansion, the complex variable method, the boundary integral equation method and the boundary element method [1].

Kung [4] studied dynamic stress concentrations resulting from the scattering of flexural waves on the thin plate with one circular hole and gave the calculations of moment and shear forces as a function of frequency. By using the flux conservation relation and optical theorem, Norris and Vemula [5] considered the scattering of flexural waves by circular inclusions with different plate properties and obtained numerical results. Squire and Dixon [6] applied the wave function expansion method to study the scattering properties of a single coated cylindrical anomaly located in a thin plate on which flexural waves propagate. Hu *et al.* [7] employed the wave function expansion and the expanded mode coefficients to represent the flexural wave scattered by a circular hole in a semi-infinite thin plate subject to the incident wave. According to the boundary conditions, these coefficients are recessively determined, which will become complicated and unmanageable as the number of holes increases. Consequently in their recent paper involving two circular holes [8], the total scattering coefficients are used. However, the proposed formulation is applicable to the case of two holes and is not general. Recently Lee and Chen [9] proposed a semi-analytical approach to solve the flexural wave scattered by multiple holes in an infinite plate by using the null field integral equation method. In addition to the need of integration, this collocation method [9] belongs to point-matching approach instead of analytical derivation. It also increases the effort of computation since boundary nodes for collocation are required.

The Trefftz method was first presented by Trefftz

[10]. On the boundary alone, this method was proposed to construct the solution space using trial complete functions which satisfy the given differential equation [11]. Apparently, Trefftz method is categorized as the boundary-type solution such as the boundary element method (BEM) or boundary integral equation method (BIEM) which can reduce the dimension of the original problem by one and thus the number of the unknowns is much less than that of the domain type methods such as finite difference method (FDM) or finite element method (FEM). Moreover, the Trefftz formulation is regular and free of calculating improper boundary integrals. However, almost all the problems solved by using Trefftz method are limited in the simply-connected domain. An extension to problems with multiple holes, i.e. multiply-connected domain, is our concern in this paper.

The concept of multipole method to solve multiply-connected domain problems was firstly devised by Závřiska [12] and used for the interaction of waves with arrays of circular cylinders by Linton and Evans [13]. Recently, one monograph by Martin [14] used these and other methods to solve problems of the multiple scattering in acoustics, electromagnetism, seismology and hydrodynamics. However, the biHelmholtz problem with the fourth order differential equation was not mentioned therein.

This paper proposed the multipole Trefftz method to solve flexural waves scattered by multiple circular holes in an analytical way. When considering an infinite thin plate with multiple circular holes, the transverse displacement field is expressed as an infinite sum of multipoles at the center of each circular hole. Based on the addition theorem, it is transformed into the same coordinate centered at the center of one circle, where the boundary conditions are given. By matching the known boundary conditions, a coupled infinite system of simultaneous linear algebraic equations is obtained and then the scattered field can be determined according to the given incident flexural wave. Once the total field is calculated as the sum of the incident field and the scattered field, the dynamic moment concentration factor along the circular holes can be determined. Some numerical results of an infinite thin plate with three circular holes subject the incident flexural wave are presented. The effects of both the space among holes and the incident wave number on the DMCF are examined in this paper.

## 2. Problem statement of scattering of flexural wave

An infinite thin plate with  $H$  circular holes

subjected to the incident flexural wave is shown in Fig. 1, where  $H+1$  observer coordinate systems are used:  $(x_1, x_2)$  is a global plane Cartesian coordinate system centered at  $O$ ,  $(\rho_p, \phi_p)$  are  $H$  local plane polar coordinates centered at  $O_p$ ,  $p=1, \dots, H$ . The radius of the  $p$ th circular hole is denoted by  $R_p$  and  $B_p$  is its corresponding boundary.

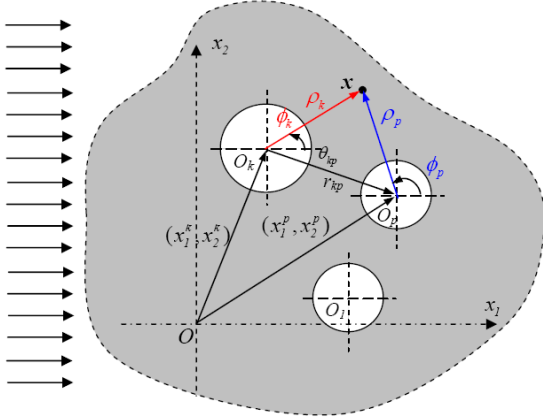


Figure 1 Problem statement for an infinite thin plate with multiple circular holes subject to an incident flexural wave

For time-harmonic motion, the governing equation of motion for the plate is

$$\nabla^4 w(\mathbf{x}) - k^4 w(\mathbf{x}) = 0, \quad \mathbf{x} \in \Omega^e, \quad (1)$$

where  $\mathbf{x}$  is the field point,  $\Omega^e$  is the unbounded exterior region occupied by the infinite plate,  $\nabla^4$  is the biharmonic operator,  $k^4 = \omega^2 \rho_0 h_0 / D$ ,  $k$  is the wave number,  $\rho_0$  is the volume density,  $h_0$  is the plate thickness,  $D = Eh_0^3 / 12(1 - \mu^2)$  is the flexural rigidity of the plate,  $E$  denotes the Young's modulus and  $\mu$  is the Poisson's ratio.

The solution of Eq. (1) in the plane polar coordinates can be represented as

$$w(\rho, \phi) = \sum_{m=-\infty}^{\infty} \tilde{w}_m(\rho) e^{im\phi}, \quad (2)$$

where  $\tilde{w}_m(\rho)$  is defined by

$$\tilde{w}_m(\rho) = \tilde{c}_1 J_m(k\rho) + \tilde{c}_2 Y_m(k\rho) + \tilde{c}_3 I_m(k\rho) + \tilde{c}_4 K_m(k\rho), \quad (3)$$

in which  $\tilde{c}_i$  ( $i=1-4$ ) are the coefficients,  $J_m$  and  $Y_m$  are the  $m$ th order Bessel functions; and  $I_m$  and  $K_m$  are the  $m$ th order modified Bessel functions. Based on the characteristics of functions at  $\rho=0$  and  $\rho \rightarrow \infty$ , the appropriate Bessel function and the modified Bessel function are chosen to represent the transverse displacement field for the infinite plate.

An incident flexural wave with an incident angle  $\alpha$  with respect to the  $x_1$  axis is represented by

$$w^{(i)}(\rho_p, \phi_p) = w_0 c_p e^{ik\rho_p \cos(\phi_p - \alpha)}, \quad p=1, \dots, H, \quad (4)$$

where  $c_p = e^{ik(x_1^p \cos \alpha + x_2^p \sin \alpha)}$  is a phase factor associated with the  $p$ th circular hole [13] of which the coordinates of the center are  $(x_1^p, x_2^p)$ . From the Jacobi's expansion [15], Eq. (4) can be expanded in a series form

$$w^{(i)}(\rho_p, \phi_p) = \sum_{m=-\infty}^{\infty} a_m^{(i)}(k\rho_p) e^{im\phi_p}, \quad p=1, \dots, H, \quad (5)$$

where  $a_m^{(i)}(k\rho_p) = w_0 c_p i^m J_m(k\rho_p) e^{-im\alpha}$ .

Based on the displacement field, the normal bending moment, tangential bending moment and effective shear force can be derived by applying the following operators with respect to the field point,

$$K_{m_n}(\cdot) = -D \left[ \mu \nabla^2(\cdot) + (1 - \mu) \frac{\partial^2(\cdot)}{\partial \rho^2} \right], \quad (6)$$

$$K_{m_t}(\cdot) = -D \left[ \nabla^2(\cdot) + (\mu - 1) \frac{\partial^2(\cdot)}{\partial \rho^2} \right], \quad (7)$$

$K_v(\cdot) =$

$$-D \left[ \frac{\partial}{\partial \rho} \left( \nabla^2(\cdot) \right) + (1 - \mu) \left( \frac{1}{\rho} \right) \frac{\partial}{\partial \phi} \left[ \frac{\partial}{\partial \rho} \left( \frac{1}{\rho} \frac{\partial(\cdot)}{\partial \phi} \right) \right] \right] \quad (8)$$

### 3. Analytical derivations for flexural wave scattered by multiple circular holes in a thin plate

Assume that a time harmonic incident flexural wave impinges on an infinite thin plate containing  $H$  circular holes as shown in Figure 1. The problem of flexural wave scattered by  $H$  circular holes is to solve Eq. (1) subject to the free traction along each circular edge and a radiation condition at infinity, i.e. the scattered field equaling to zero when  $\rho \rightarrow \infty$ . Based on Eq. (2), we can express the scattered field as an infinite sum of multipoles at the center of each hole as follows:

$$w^{sc}(\mathbf{x}; \rho_1, \phi_1, \dots, \rho_H, \phi_H) = \sum_{k=1}^H \left[ \sum_{m=-\infty}^{\infty} a_m^k H_m^{(1)}(k\rho_k) e^{im\phi_k} + b_m^k K_m(k\rho_k) e^{im\phi_k} \right], \quad (9)$$

where  $(\rho_1, \phi_1), \dots, (\rho_H, \phi_H)$  are the polar coordinates of the field point  $\mathbf{x}$  with respect to each center of holes. The Hankel function ( $J+iY$ ) and the modified Bessel function  $K$  are chosen to represent the infinite plate due to their values being finite as  $\rho \rightarrow \infty$ . The coefficients of  $a_m^k$  and  $b_m^k$ ,  $k=1, \dots, H$ ;  $m=0, \pm 1, \pm 2, \dots$ , are determined by matching the boundary condition on each circle. To satisfy the specified boundary conditions, the total field is required and defined by

$$w(\mathbf{x}) = w^{(i)}(\mathbf{x}) + w^{sc}(\mathbf{x}). \quad (10)$$

By combining Eq.(5) and Eq.(9), the total displacement field is explicitly represented by

$$\begin{aligned} & w(\mathbf{x}; \rho_1, \phi_1, \dots, \rho_H, \phi_H) \\ &= \sum_{m=-\infty}^{\infty} a_m^{(i)}(k\rho_p) e^{im\phi_p} + \\ & \sum_{k=1}^H \left[ \sum_{m=-\infty}^{\infty} a_m^k H_m^{(1)}(k\rho_k) e^{im\phi_k} + b_m^k K_m(k\rho_k) e^{im\phi_k} \right], \quad (11) \\ & p = 1, \dots, H. \end{aligned}$$

In the following, we are mainly concerned with the free traction condition for each circular edge. The bending moment and shear force along each hole,  $p=1, \dots, H$ , can be obtained by substituting Eq. (11) into Eqs. (6) and (8). The unknown coefficients of  $a_m^k$  and  $b_m^k$  can be determined through the following boundary conditions,  $0 \leq \phi_p \leq 2\pi$ ,  $\rho_p = R_p$ ,  $p = 1, \dots, H$ ,

$$m_n(\rho_p, \phi_p) = 0, \quad (12)$$

$$v(\rho_p, \phi_p) = 0. \quad (13)$$

But it is difficult to determine the unknown coefficients by using the procedure mentioned above. This question can be answered by using the addition theorem [15] which will be described in the following.

Based on the Graf's addition theorem for the Bessel functions, we can express the theorem in the following form,

$$J_m(k\rho_k) e^{im\phi_k} = \sum_{n=-\infty}^{\infty} J_{m-n}(kr_{kp}) e^{i(m-n)\theta_{kp}} J_n(k\rho_p) e^{in\phi_p}, \quad (14)$$

$$I_m(k\rho_k) e^{im\phi_k} = \sum_{n=-\infty}^{\infty} I_{m-n}(kr_{kp}) e^{i(m-n)\theta_{kp}} I_n(k\rho_p) e^{in\phi_p}, \quad (15)$$

$$H_m^{(1)}(k\rho_k) e^{im\phi_k} = \begin{cases} \sum_{n=-\infty}^{\infty} H_{m-n}^{(1)}(kr_{kp}) e^{i(m-n)\theta_{kp}} J_n(k\rho_p) e^{in\phi_p}, & \rho_p < r_{kp}, \\ \sum_{n=-\infty}^{\infty} J_{m-n}(kr_{kp}) e^{i(m-n)\theta_{kp}} H_n^{(1)}(k\rho_p) e^{in\phi_p}, & \rho_p > r_{kp}, \end{cases} \quad (16)$$

$$K_m(k\rho_k) e^{im\phi_k} = \begin{cases} \sum_{n=-\infty}^{\infty} (-1)^n K_{m-n}(kr_{kp}) e^{i(m-n)\theta_{kp}} I_n(k\rho_p) e^{in\phi_p}, & \rho_p < r_{kp}, \\ \sum_{n=-\infty}^{\infty} (-1)^{m-n} I_{m-n}(kr_{kp}) e^{i(m-n)\theta_{kp}} K_n(k\rho_p) e^{in\phi_p}, & \rho_p > r_{kp}, \end{cases} \quad (17)$$

where  $(\rho_p, \phi_p)$  and  $(\rho_k, \phi_k)$  as shown in Figure 1 are the polar coordinates of the field point  $\mathbf{x}$  with respect to  $O_p$  and  $O_k$ , respectively, which are the origins of two polar coordinate systems and  $(r_{kp}, \theta_{kp})$  are the polar coordinates of  $O_p$  with respect to  $O_k$

By substituting the addition theorem for the Bessel functions  $H_m^{(1)}(k\rho_k)$  and  $K_m(k\rho_k)$  into Eq. (11),

the displacement field near the circular boundary  $B_p$  for the case of  $\rho_p < r_{kp}$  is given by

$$\begin{aligned} w(\mathbf{x}; \rho_p, \phi_p) &= \sum_{m=-\infty}^{\infty} e^{im\phi_p} \{ a_m^{(i)}(k\rho_p) \\ &+ H_m^{(1)}(k\rho_p) a_m^p + K_m(k\rho_p) b_m^p \\ &+ \sum_{k=1}^H \left[ \sum_{n=-\infty}^{\infty} A_{mn}^k(k\rho_p) a_n^k + B_{mn}^k(k\rho_p) b_n^k \right] \}, \quad (18) \end{aligned}$$

where

$$A_{mn}^k(k\rho_p) = H_{n-m}^{(1)}(kr_{kp}) e^{i(n-m)\theta_{kp}} J_m(k\rho_p), \quad (19)$$

$$B_{mn}^k(k\rho_p) = (-1)^m e^{i(n-m)\theta_{kp}} K_{n-m}(kr_{kp}) I_m(k\rho_p). \quad (20)$$

By substituting Eq. (18) into Eq. (6), the normal bending moment,  $m_n(x)$ , near the circular boundary  $B_p$  ( $p=1, \dots, H$ ) is given by

$$\begin{aligned} m_n(\mathbf{x}; \rho_p, \phi_p) &= \sum_{m=-\infty}^{\infty} e^{im\phi_p} \{ c_m^{(i)}(k\rho_p) \\ &+ \alpha_m^H(k\rho_p) a_m^p + \alpha_m^K(k\rho_p) b_m^p \\ &+ \sum_{k=1}^H \left[ \sum_{n=-\infty}^{\infty} C_{mn}^k(k\rho_p) a_n^k + D_{mn}^k(k\rho_p) b_n^k \right] \}, \quad (21) \end{aligned}$$

where

$$C_{mn}^k(k\rho_p) = H_{n-m}^{(1)}(kr_{kp}) e^{i(n-m)\theta_{kp}} \alpha_m^J(k\rho_p), \quad (22)$$

$$D_{mn}^k(k\rho_p) = (-1)^m e^{i(n-m)\theta_{kp}} K_{n-m}(kr_{kp}) \alpha_m^I(k\rho_p), \quad (23)$$

$$c_m^{(i)}(k\rho_p) = c_p^i \alpha_m^J(k\rho_p) e^{-ima}. \quad (24)$$

The moment operator  $\alpha_m^X$  from Eq. (6) is defined as follows:

$$\alpha_m^X(k\rho) = D \left\{ (1-\mu) \frac{X'_m(k\rho)}{\rho} - \left[ (1-\mu) \frac{m^2}{\rho^2} \mp k^2 \right] X_m(k\rho) \right\}, \quad (25)$$

where the upper (lower) signs refer to  $X = J, Y, H, (I, K)$ , respectively. The second order differential equations for these functions have been used to simplify  $\alpha_m^X(k\rho)$ .

Similarly, the effective shear operator  $\beta_m^X$  derived from Eq. (8) can be expressed as

$$\beta_m^X(k\rho) = D \left\{ \left[ m^2(1-\mu) \pm (k\rho)^2 \right] \frac{X'_m(k\rho)}{\rho^2} - m^2(1-\mu) \frac{X_m(k\rho)}{\rho^3} \right\} \quad (26)$$

and the field of effective shear,  $v(x)$ , near the circular boundary  $B_p$  ( $p=1, \dots, H$ ) is given by

$$v(\mathbf{x}; \rho_p, \phi_p) = \sum_{m=-\infty}^{\infty} e^{im\phi_p} \{ d_m^{(i)}(k\rho_p) + \beta_m^H(k\rho_p)a_m^p + \beta_m^K(k\rho_p)b_m^p + \sum_{\substack{k=1 \\ k \neq p}}^H \left[ \sum_{n=-\infty}^{\infty} E_{mn}^k(k\rho_p)a_n^k + F_{mn}^k(k\rho_p)b_n^k \right] \}, \quad (27)$$

where  $E_{mn}^k(k\rho_p)$ ,  $F_{mn}^k(k\rho_p)$  and  $d_m^{(i)}(k\rho_p)$  are obtained by replacing  $\alpha_m^X(k\rho_p)$  in Eqs. (22)–(24) with  $\beta_m^X(k\rho_p)$ , respectively.

According to the traction-free conditions of Eqs. (12) and (13), applying the orthogonal property of  $\{e^{im\phi_p}\}$  to Eqs.(21) and (27), respectively, and setting  $\rho_p$  to  $R_p$  give

$$\begin{cases} \alpha_m^H(kR_p)a_m^p + \alpha_m^K(kR_p)b_m^p + \sum_{\substack{k=1 \\ k \neq p}}^H \left[ \sum_{n=-\infty}^{\infty} C_{mn}^k(kR_p)a_n^k + D_{mn}^k(kR_p)b_n^k \right] = -c_m^{(i)}(kR_p) \\ \beta_m^H(kR_p)a_m^p + \beta_m^K(kR_p)b_m^p + \sum_{\substack{k=1 \\ k \neq p}}^H \left[ \sum_{n=-\infty}^{\infty} E_{mn}^k(kR_p)a_n^k + F_{mn}^k(kR_p)b_n^k \right] = -d_m^{(i)}(kR_p), \end{cases} \quad (28)$$

for  $m=0, \pm 1, \pm 2, \dots$ ,  $n=0, \pm 1, \pm 2, \dots$ , and  $p = 1, \dots, H$ . Equation (28) is a coupled infinite system of simultaneous linear algebraic equations which is the analytical model for the flexural scattering of an infinite plate containing multiple holes. In order to evaluate the numerical results in the following section, the infinite system of Eq. (28) is truncated to a  $(2H) \times (2M+1)$  system of equations for  $(2H) \times (2M+1)$  unknown coefficients, i.e.  $m=0, \pm 1, \pm 2, \dots, \pm M$ . Once the coefficients  $a_m^k$  and  $b_m^k$  ( $k=1, \dots, H$ ;  $m=0, \pm 1, \pm 2, \dots, \pm M$ ) are determined, the total field of displacement, the bending moment and the shear force can be obtained by substituting them into Eqs. (11), (21) and (27).

In the polar coordinates, the normal bending moment, tangential bending moment and effective shear force induced by the incident wave can be determined by substituting Eq. (4) into Eqs. (6)–(8). By setting the amplitude of incident wave to be one ( $w_0 = 1$ ), the amplitude of normal bending moment produced by the incident wave is

$$M_0 = Dk^2. \quad (29)$$

The dynamic moment concentration factor (DMCF) at any field point  $\mathbf{x}$  is defined as

$$\text{DMCF}(\mathbf{x}) = m_t(\mathbf{x}) / M_0, \quad (30)$$

where the tangential bending moment  $m_t(\mathbf{x})$  is

determined by substituting Eq. (18) into Eq.(7) with respective to the field point as follows:

$$m_t(\mathbf{x}; \rho_p, \phi_p) = \sum_{m=-\infty}^{\infty} e^{im\phi_p} \{ f_m^{(i)}(k\rho_p) + \gamma_m^H(k\rho_p)a_m^p + \gamma_m^K(k\rho_p)b_m^p + \sum_{\substack{k=1 \\ k \neq p}}^H \left[ \sum_{n=-\infty}^{\infty} G_{mn}^k(k\rho_p)a_n^k + H_{mn}^k(k\rho_p)b_n^k \right] \}, \quad (31)$$

where  $G_{mn}^k(k\rho_p)$ ,  $H_{mn}^k(k\rho_p)$  and  $f_m^{(i)}(k\rho_p)$  are obtained by replacing  $\alpha_m^X(k\rho_p)$  in Eqs. (22)–(24) with  $\gamma_m^X(k\rho_p)$ , respectively, and the tangential bending moment operator  $\gamma_m^X(k\rho)$  derived from Eq. (7) is given by

$$\gamma_m^X(k\rho) = D \left\{ (\mu-1) \frac{X_m'(k\rho)}{\rho} - \left[ (\mu-1) \frac{m^2}{\rho^2} \mp \mu k^2 \right] X_m(k\rho) \right\}. \quad (32)$$

#### 4. Numerical results and discussions

To demonstrate the validity of the proposed method, the FORTRAN code was implemented to solve the flexural wave scattered by three circular holes shown in Fig 2, where  $L$  denotes the central distances between holes. The coordinates of three holes are  $(\sqrt{3}L/2, 0)$ ,  $(0, L/2)$  and  $(0, -L/2)$ , respectively. The DMCF around the circular hole is determined since it is important to the structure design such as fatigue failure evaluation. In all cases, all edges of holes are subjected to the traction-free boundary conditions and the thickness of plate is 0.002m. To obtain the more accurate results, numerical experiments show that the required number of  $M$  truncated in the finite system mainly depends on the minimum dimensionless central distance  $L/a$  to be considered. Through the numerical experiments, it is found that the required number of  $M$  can be taken from 20 to 8 for the minimum separation distance  $L/a$  ranged from 2.1 to 10.0. Only when does the value of  $L/a$  become large such as 4.0 or 10.0, the required number of  $M$  is related to the incident wave number. In other words, the required number of  $M$  to the convergence increase as the incident wave number becomes larger.

Figures 3–6 show the distribution of DMCF on the first and the second circular boundary  $B_1$  and  $B_2$ , respectively, when three different incident dimensionless wave numbers ( $ka=0.5, 1.0$  and  $3.0$ ) and three different dimensionless central distance ( $L/a=2.1, 2.5$  and  $4.0$ ) are considered. The

distribution of DMCF on the third circular boundary  $B_3$  is equal to that on the second one due to the symmetry of the  $x_1$ -axis, so that it is not presented here. It can be observed that the distribution of DMCF of three circular holes is different from that of one, where the maximum of DMCF occurs at  $\phi = \pi/2$  and  $-\pi/2$  when the incident wave number is small and the incident angle equals to zero.

In addition to the incident wave number, the distribution of DMCF apparently depends on two factors. One is the geometry and the other is the angle of the incident wave. Since the first circular hole is located near the other circular holes at  $\phi = 5\pi/6$  and  $-5\pi/6$  where the separated space is very small and meanwhile the incident wave is from the negative of the  $x_1$  axis, the maximum of DMCF on the boundary of the first hole occurs at  $\phi = \pi/2, 5\pi/6, -5\pi/6,$  and  $-\pi/2$  as shown in Fig. 3. As the value of  $ka$  increases, the factor of geometry is obviously amplified but that of incident angle is attenuated a little. Figure 4 shows that the maximum of DMCF on the boundary of the second hole occurs at  $\phi = -\pi/2$  and  $-\pi/6$ . The maximum of DMCF at  $\phi = -\pi/6$  is similar to those of the first hole. But the maximum of DMCF at  $\phi = -\pi/2$  is the largest of all considered so far because two factors simultaneously occur at this point: the narrow space and the incident flexural wave with  $\alpha = 0$ .

As the dimensionless central distance  $L/a$  increases to 2.5 and 4.0 as shown in Figs.5-6, the DMCF gradually decreases since the geometry factor is attenuating. Meanwhile the shadow on the first hole coming from the other holes gradually decreases so that the more incident wave impinges on the first holes. According, the magnitude of DMCF of the first hole at  $\phi = \pi/2$  and  $-\pi/2$  becomes large instead of decreasing as shown in Figs. 3, 5 and 6.

Figures 7-8 show DMCF on the first and the second circular boundaries at  $\phi = -\pi/2$  as a function of the dimensionless incident wave number at four different dimensionless central distances, dotted line for  $L/a = 2.1$ , dashed line for  $L/a = 2.5$ , dot-dashed line for  $L/a = 4.0$  and solid line for  $L/a = 10.0$ . It can be seen from Fig.7 that the DMCF on the first circular boundary at  $\phi = -\pi/2$  is apparently related to the space between holes when the incident wave number is small. Because of the shadow effect, the smaller the central distance is ; the smaller the DMCF is. This effect is gradually replaced by that of the multiple scattering as the incident wave number  $ka$  increases. Instead of the

incident wave number, the geometry factor dominates the DMCF on the second circular boundary at  $\phi = -\pi/2$  as shown in Fig. 10. It can be seen that when space is large enough such as  $L/a=10.0$  and  $ka$  approaches zero, the value of DMCF approaches 1.85 which agrees with the analytical solution of an infinite plate with one hole [1]. As the value of  $ka$  increases, the magnitude of DMCF becomes more fluctuated especially for the case of the large value of  $L/a$ .

Figures 9-10 show DMCF on the first and the second circular boundaries at  $\phi = -\pi/2$  as a function of the dimensionless central distance at three different dimensionless incident wave numbers, dotted line for  $ka = 0.5$ , dashed line for  $ka = 1.0$  and solid line for  $ka = 3.0$ . It can be seen from Fig. 9 that the shadow effect at the low incident wave number is rapidly released as the separation distance increases. Comparing Figs 9 and 10, even though two plots varied in the different way, these variations will converge to the same level as the value of  $L/a$  approaches to infinite. It can be seen from Figs. 9-10 that for the high incident wave number the DMCF shows obvious oscillation as the space among holes varies. Actually, this oscillation exists in all cases of the incident wave number and the detail can be seen in the recent paper of [9].

## 5. Concluding remarks

The flexural wave scattered by multiple circular holes in a thin plate has been theoretically solved by using the multipole Trefftz method with the aid of the addition theorem. By using the addition theorem, the Trefftz method can be extended to deal with multiply-connected domain problems. The proposed algorithm is general and easily applicable to problems with multiple holes which are not easily solved by using the traditional analytical method. By matching boundary conditions, the analytical model for the multiple scattering of the plate problem can be derived as a coupled infinite system of simultaneous equations. An example of an infinite plate containing three holes in a truncated system is presented and the effects of the central distance and the incident wave number on the dynamic moment concentration factor (DMCF) are investigated in this paper. The distribution of DMCF of three holes is significantly different that of one. The geometry factor mainly affects the DMCF especially under the specified direction of incident wave.

## 6. References

- [1] Pao, Y. H. and Mow, C. C., Diffraction of elastic waves and dynamics stress concentration, Crane-Russak, New York, 1972.
- [2] Nishimura, G. and Jimbo, Y., "A dynamical problem of stress concentration", Journal of the Faculty of Engineering, University of Tokyo, Japan, vol. 24, pp.101-, 1955.
- [3] Pao, Y. H., "Dynamical stress concentration in an elastic plate", Transactions of the ASME Journal of Applied Mechanics, vol. 29, pp. 299-305, 1962.
- [4] Kung, George C. S., Dynamical stress concentration in an elastic plate. M.S. Thesis, Cornell University, Ithaca, New York, 1964.
- [5] Norris, A. N. and Vemula, C., "Scattering of flexural waves on thin plates", Journal of Sound and Vibration, vol. 181, pp.115-125, 1955.
- [6] Squire V. A. and Dixon, T. W., "Scattering of flexural waves from a coated cylindrical anomaly in a thin plate", Journal of Sound and Vibration, vol. 236, no.2, pp. 367-373, 2000.
- [7] Hu, C., Fang, X. Q. and Huang, W. H., "Multiple scattering of flexural waves in a semi-infinite thin plate with a cutout", International Journal of Solids and Structures, vol. 44, pp. 436-446, 2007.
- [8] Fang, X. Q., Hu, C. and Wang, D. B., "Multiple scattering of flexural waves from two cutouts in a semi-infinite thin plate", International Journal of Solids and Structures, vol. 45, pp. 4236-4246, 2008.
- [9] Lee, W. M. and Chen, J. T., "Scattering of flexural wave in thin plate with multiple holes by using the null-field integral equation approach. CMES-Computer Modeling in Engineering & Sciences", vol.37, no.3, 243-273, 2008.
- [10] Trefftz, E., "Ein Gegenstück zum Ritz' schen Verfahren", Proc. Second Int. Cong. Appl. Mech., Zurich, pp. 131-137, 1926.
- [11] Kamiya, N. and Kita, E., "Trefftz method: an overview", Advances in Engineering Software, vol. 24, pp.3-12, 1955.
- [12] Závřiska, F., "Über die Beugung elektromagnetischer Wellen an parallelen, unendlich langen Kreiszyllindern", Annalen der Physik, 4 Folge, vol. 40, pp. 1023-1056, 1913.
- [13] Linton, C. M. and Evans, D. V., "The interaction of waves with arrays of vertical circular cylinders", Journal of Fluid Mechanics, vol. 215, pp. 549-569, 1999.
- [14] Martin, P. A., Multiple scattering interaction of time-harmonic wave with N obstacles, Cambridge University Press, Cambridge, 2006.
- [15] Watson, G. N., A Treatise on the Theory of Bessel Functions, second edition. Cambridge: Cambridge Library edition, 1995.

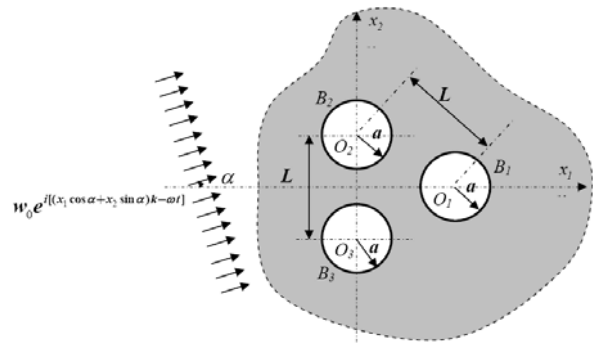


Figure 2 An infinite thin plate with three circular holes subject to an incident flexural wave

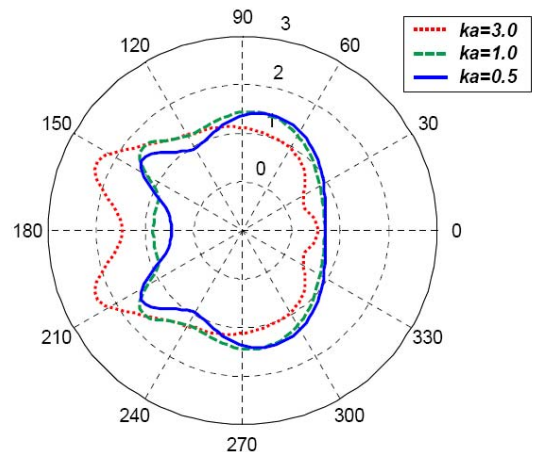


Figure 3 Distribution of DMCF on the  $B_1$  at three different dimensionless wave numbers, solid line for  $ka = 0.5$ , dashed line for  $ka = 1.0$  and dotted line for  $ka = 3.0$  ( $L/a = 2.1$ )

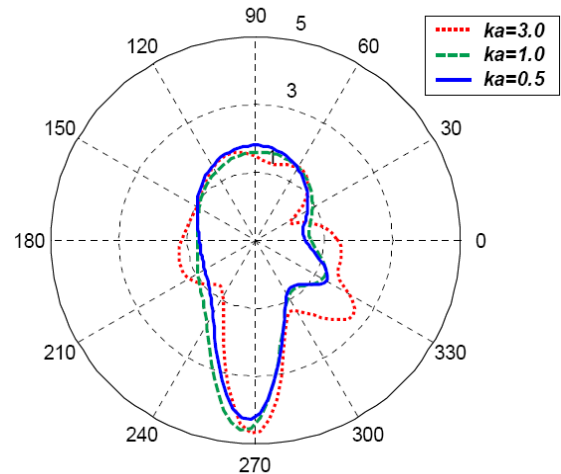


Figure 4 Distribution of DMCF on the  $B_2$  at three different dimensionless wave numbers, solid line for  $ka = 0.5$ , dashed line for  $ka = 1.0$  and dotted line for  $ka = 3.0$  ( $L/a = 2.1$ )

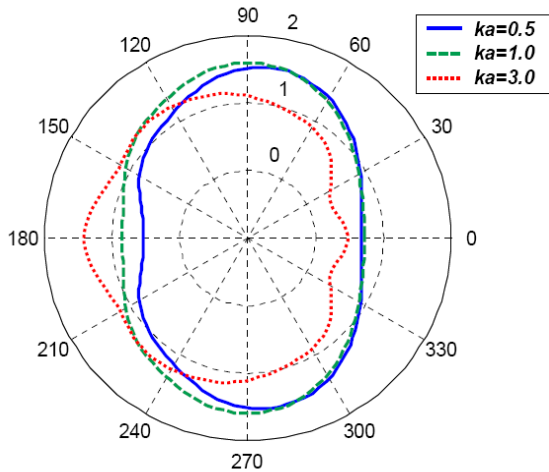


Figure 5 Distribution of DMCF on the  $B_1$  at three different dimensionless wave numbers, solid line for  $ka = 0.5$ , dashed line for  $ka = 1.0$  and dotted line for  $ka = 3.0$  ( $L/a = 2.5$ )

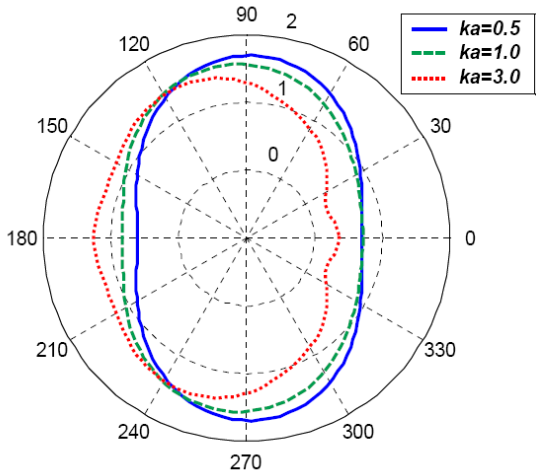


Figure 6 Distribution of DMCF on  $B_1$  at three different dimensionless wave numbers, solid line for  $ka = 0.5$ , dashed line for  $ka = 1.0$  and dotted line for  $ka = 3.0$  ( $L/a = 4.0$ )

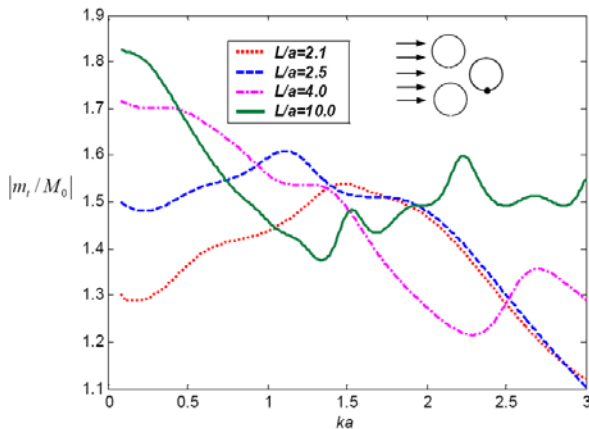


Figure 7 DMCF on the  $B_1$  ( $\phi = -\pi/2$ ) versus the dimensionless wave number at four different dimensionless central distances, dotted line for  $L/a = 2.1$ , dashed line for  $L/a = 2.5$ , dot-dashed line for  $L/a = 4.0$  and solid line for  $L/a = 10.0$

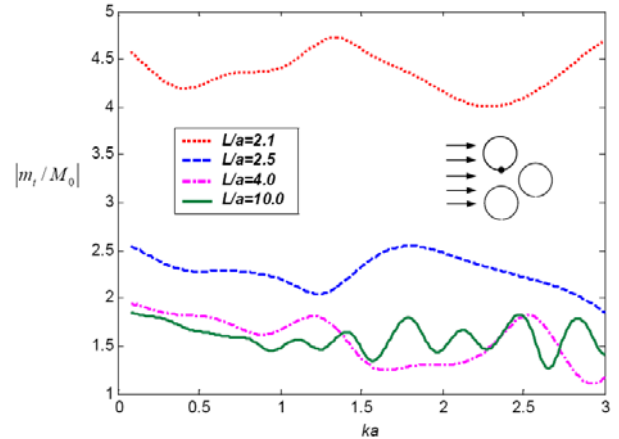


Figure 8 DMCF on the  $B_2$  ( $\phi = -\pi/2$ ) versus the dimensionless wave number at four different dimensionless central distances, dotted line for  $L/a = 2.1$ , dashed line for  $L/a = 2.5$ , dot-dashed line for  $L/a = 4.0$  and solid line for  $L/a = 10.0$

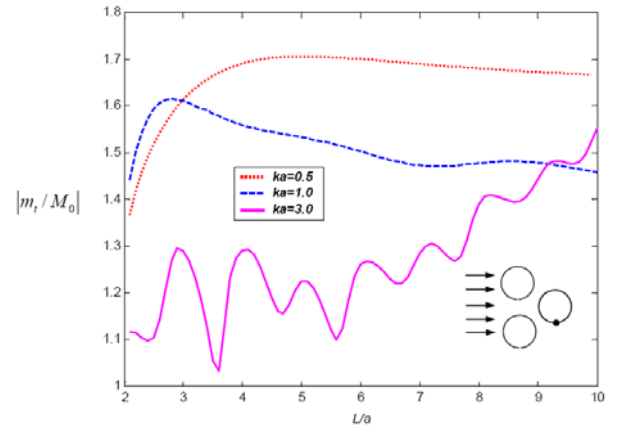


Figure 9 DMCF on the  $B_1$  ( $\phi = -\pi/2$ ) versus the dimensionless central distance at three different dimensionless wave numbers, dotted line for  $ka = 0.5$ , dashed line for  $ka = 1.0$  and solid line for  $ka = 3.0$

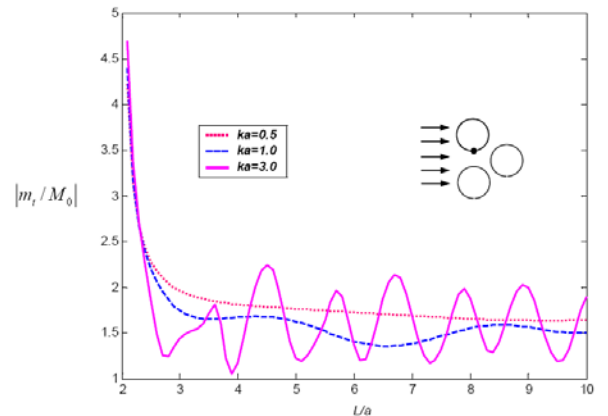


Figure 10 DMCF on the  $B_2$  ( $\phi = -\pi/2$ ) versus the dimensionless central distance at three different dimensionless wave numbers, dotted line for  $ka = 0.5$ , dashed line for  $ka = 1.0$  and solid line for  $ka = 3.0$